Dakka *et al.*
Journal of Engineering and Applied Science (2024) 71:7
https://doi.org/10.1186/s44147-023-00333-2

Journal of Engineering and Applied Science

RESEARCH Open Access

A 5-kW unidirectional wireless power transfer EV charger with a novel multi-level PFC boost converter on front-end side

Obulesu Dakka[1], Sridhar Patthi[2], J. V. G. Rama Rao[3] and Parveen Kumar[4*]

*Correspondence:
parveenrao423@gmail.com

[1] Department of Electrical Engineering, CVR College of Engineering, Ibrahimpatnam 501510, India
[2] Department of Electrical Engineering, Institute of Aeronautical Engineering, Hyderabad 500043, India
[3] Department of Electrical Engineering, BVC Institute of Technology and Science, Amalapuram 533221, India
[4] Department of Electrical Engineering, Model Institute of Engineering and Technology (MIET), Jammu 181122, India

Abstract

The greatest advantages of wireless power transfer (WPT) are its absence of severe environmental hazards, its portability, and its independence from other factors. The wireless charging system for electric vehicles has a serious problem with the amount of misalignment it can tolerate. This study explores the usage of a novel multi-level boost power factor correction (PFC) rectifier with less switch count to improve the efficiency of power conversion of a 5-kW wireless electric vehicle (EV) charger. Especially in the context of wireless charging, which provides convenience and flexibility, there is a pressing need for efficient and dependable charging infrastructure to keep up with the rising demand for electric vehicles. In contrast to wired EV chargers, wireless chargers often have poorer power conversion efficiency because of losses in power semiconductor devices. An innovative multi-level boost PFC rectifier design is offered as a solution to this problem since it uses fewer switches while retaining high-performance levels. The suggested rectifier achieves much higher power conversion efficiency. In addition, power factor correction capabilities are improved, making it comply with global rules. Simpler, cheaper, and more dependable rectifiers improve the whole system.

Keywords: Wireless charge, Receiver coils, Multi-level boost PFC rectifier, Power factor correction, Total harmonic distortion

Introduction

The advent of widespread electricity generation has resulted in a new era of social and economic development and environmental development. As the focus moves from the energy transition to a carbon-neutral emission economy, electrification is projected to increase in the transportation sector. In order to mitigate climate change, greenhouse gas emissions, and poor air quality, electrifying transportation is seen as a promising alternative to traditional fuel sources. When compared to cars powered by traditional internal combustion engines (ICE), EVs have several advantages, including zero emissions, high reliability, high efficiency, and little maintenance. More than 10 million EVs were on the road in 2020, and market research predicts that number will grow to over one billion EVs by 2050 [1]. All of these things have an effect on the auto

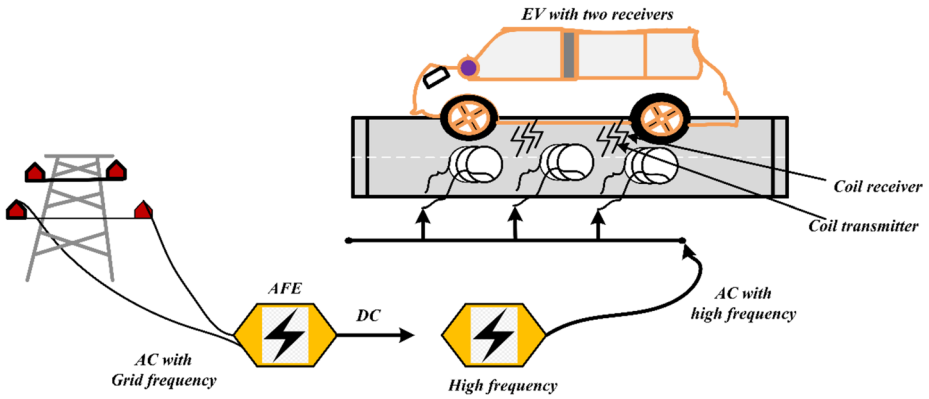

Fig. 1 Wireless EV power transmission system

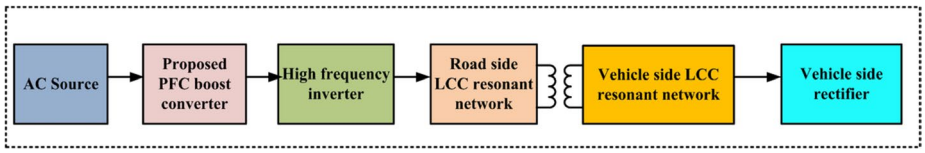

Fig. 2 Block diagram of wireless power transfer

industry and are crucial to the study and improvement of electric vehicle (EV) technology. In recent years, wireless power transfer, also known as WPT, has been gaining a lot of attention [2, 3].

It finds extensive use in several fields, including the transportation sector [4–6], the consumer electronics industry [7, 8], the home and kitchen and the transportation of goods [9, 10]. Without physical touch between the sending and receiving sides, energy is transferred through the coupled magnetic field in a WPT system [9]. In the present day, electric vehicles may be charged using either an active wired power transfer system or a wireless power transfer system (WPT) [10]. This research explores a specific kind of WPT device known as active power wireless power transfer. Although numerous methods exist for WPT, the most developed ones use induction [11]. This kind of charger relies on an 80–90 kHz magnetic field running between two air-core linked coils. Wireless chargers power converters vary from their wired counterparts in composition, architecture, and control due to their operating frequency. The typical wireless EV system is depicted in Fig. 1.

In [12], the various types of power converters used in two-way wired as well as wireless chargers are discussed. Regarding management, a comparison is provided in [13] between two primary approaches to managing the flow of power in bidirectional wireless chargers. The onboard charging (OBC) system should be more efficient, affordable, and grid friendly, as well as have a higher-power density, higher-energy utilization, a smaller form factor, less weight, and higher reliability [14]. Based on the number of steps used to process power, the typical OBC topologies may be roughly divided into two classes: two-stage and single-stage chargers [15]. As shown in Fig. 2, the typical two-stage setups include a front-end AC-DC converter consisting of a diode bridge rectifier with power factor correction (PFC) and an isolated DC-DC converter, as described in [16].

In order to regulate the output voltage, two-stage chargers utilize a DC-DC converter at the conclusion of the charging process [17] and an AC-DC converter at the beginning of the charging process for active power factor correction (PFC). It is recommended to use a two-stage EV charger that combines a modified buck-boost converter and a half-bridge LLC converter [18]. As a practical front-end converter for OBC, a single-phase switched-mode bridge-less AC-DC buck-boost-derived converter is presented [19]. The suggested converter has fewer moving parts and fewer sensors, which helps keep the charger cost down. To improve PFC converters, which do not need extra sample devices, a system for online capacitance monitoring was presented [20]. The converters on the back end have no effect on the proposed design.

The ripples in the steady state are small, but the transient duration is excessively lengthy [21]. debuted the FR series of bridgeless PFC rectifiers, which consists of two new single-phase buck-boost designs. Both suggested rectifiers use just two semiconductors and a single magnetic core to power two inductors. In this study, we present a PFC rectifier design that makes use of fewer active switches but yet achieves multi-level PFC boost power factor correction. The smaller number of switches also helps to reduce the overall footprint of the manufacturing box. The switches in the rectifier are subjected to low-voltage strains and work at low switching frequencies, making the device ideal for medium-voltage high-power applications. This rectifier's ability to produce Dc voltage and current with minimal harmonic content is a major benefit. This attribute is greatly sought after in power electronic systems due to its beneficial effects on enhancing power quality and decreasing distortion. The multi-level converter design used in the rectifier makes these advantages possible.

In PFC converter design voltage stability is an important parameter to manage the power from vehicle to grid and grid to vehicle [22]. presents an improved version of the particle swarm optimization technique for online power system stabilizer tuning. The program uses an innovative objective function that combines angular velocity deviation and damping time measurements. Simulations show greater oscillation mitigation under varied power system load circumstances as compared to genetic and bacterial foraging algorithms. The effectiveness of STATCOM, TCSC, SSSC, and UPFC in improving the static voltage stability of the IEEE 14-bus test system is evaluated in [23].

The study of the continuation power flow and the saddle node bifurcation demonstrates the way their effects appear at the highest loading point. The holistic power transfer in [24] presents a probabilistic technique to analyze distant wind power supply dependability to the main grid, including transmission restrictions. It calculates transmission capacity for system dependability and cost-effectiveness using the mean capacity outage probability table (mean-COPT) paradigm, which considers fuel offset and environmental advantages. The illustrations incorporate real wind farm data, which helps electricity system planners and regulators. In [25], research optimizes microgrid controller settings for islanding mode using particle swarm optimization (PSO) to minimize current and voltage controller faults and simulate stability. To improve voltage stability, [26] deliberately places wind generating at power system weak areas. It emphasizes static VAR compensators with maximum loading factor and megawatt margin indicators. Simulations using the IEEE 14-bus test system support the method.

The optimization of reactive power compensation in the IEEE 30-bus system for voltage stability and cost savings is presented in [27]. The Modified Artificial Bee Colony surpasses Artificial Bee Colony, PSO, and GA in losses, reactive power costs, voltage profile, and system stability. An optimal fuzzy-based controller for autonomous generation regulation in a wind farm-connected two-area hydrothermal power system approaches modified cuckoo search optimization controller settings and membership functions. The suggested heuristic goal function emphasises maximum frequency drift and oscillations fading time to minimize frequency deviation and transmission power oscillations. The wind farm's load changes and contribution to fulfilling electrical demand minimize frequency oscillations in both locations, improving power system stability in simulations [28].

The high switching frequency of multi-level converters is addressed in this study by using a four-carrier pulse-width modulation (PWM) approach. Because of its usefulness in managing power electronic converters, this method has found widespread use in industry. A simple cascaded controller is used to provide the PWM modulation reference signal. For the novel PFC boost rectifier converter, this controller's voltage and current loops coordinate to regulate the DC voltage at the output, maintain phase between the input voltage and current, and produce a voltage waveform with five levels. The study includes extensive test results that demonstrate the effective operation of the suggested rectifier.

However, the arrangement itself may not be suitable for use in industrial applications. So, that multi-level PFC converter is connected to wireless power transfer converter which provides isolation. Overall, this novel PFC-based wireless converter excels in efficiency indices, which are crucial to EV charger performance. It offers more efficiency than other similar-level PFC-based EV chargers due to careful design and control strategy. This converter outperforms previous works in terms of power factor, component count, and efficiency, making it a desirable choice for eco-friendly EV battery charging. The output DC voltage, power factor, harmonic current, and operating frequency of the rectifier were all confirmed to be low ripple by testing. The suggested multi-carrier PWM method and the straightforward controller both enhance the rectifier usefulness and efficiency. Using the LCC network and the proposed PFC boost converter describes the two-stage, unidirectional wireless transmission of power using the MATLAB/Simulink simulation environment. The remaining part of the article covers the results of the simulation.

Mathematical model of the wireless charging system

Wireless charging is becoming more common on highways since it extends the range of electric cars (EVs), especially pure and hybrid EVs. However, the wireless charge method is particularly useful for battery electric vehicles (BEVs) since it offers a method for recharging the vehicle even while it is in motion. This makes the wireless recharge method an attractive option for BEV manufacturers. There is a basic essence that can be found inside the arena of electric vehicles (EVs), which gives these cars their own existence and gives them life. At its center is the mysterious component that is often referred to as the battery.

As shown in Fig. 3, it stands a dominant DC voltage source, also prominently featuring the design of this normal entity. This DC voltage source is enveloped by a balanced number of series variable resistances. This ensemble with numerous parameters, each delicately tangled in Eq. (1) [29–33], an enchantment that unveils the charge/discharge voltage characteristics of the enigmatic lithium-ion battery. This enigmatic equation manages to encapsulate the very essence of this component, thereby illuminating its enigmas and setting the stage for a captivating exploration of battery voltage (U_{batt}). The internal resistance of battery (R_{batt}) influences the battery charging and discharging ($U_{batt\text{-}charge}$ and $U_{batt\text{-}discharge}$) phenomena.

$$U_{batt} = \begin{cases} U_{batt-ch\arg e} = E_b^I - R_{batt} I_{batt} \\ U_{batt-dich\arg e} = E_b^I - R_{batt} I_{batt} \end{cases} \tag{1}$$

q(t) is the time-integral of the battery's remaining capacity, and it is expressed as follows:

$$q(t) = q(0) - \int_0^{t_{batt}} (\eta_{batt} I_{batt}) dt \tag{2}$$

Here, t_{batt} is the discharge time and battery current (I_{batt}) and η_{batt} is battery performance are primary elements considered in wireless charging system. The SoC of the system at q_{max} can be represented as follows:

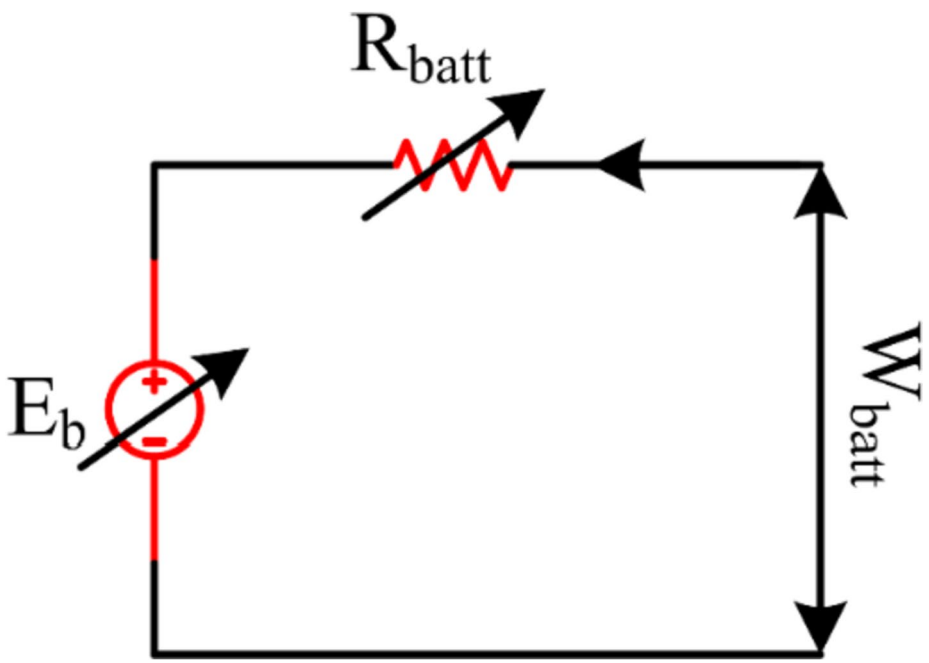

Fig. 3 Li-ion battery equivalent circuit

$$SoC(\%) = \left(\frac{q(t)}{q_{\max}}\right) \times 100 \tag{3}$$

The internal components of battery are determining its discharge and charge voltage (E_b^I), which can be expressed as follows:

$$E_b^I = \begin{cases} E_0 - K_b\left(\frac{q}{q-it}\right) i_{ld} * -K_b\left(\frac{q}{q-it}\right) it + Ae^{-B.it} \\ E_0 - K_b\left(\frac{q}{q-it}\right) i_{ld} * +K_b\left(\frac{q}{q-it}\right) it + Ae^{-B.it} \end{cases} \tag{4}$$

Here, the constant voltage is denoted by E_0, the polarization resistance by K_b, $i_{ld}{}^*$ represents the low-frequency current dynamics, the extracted capacity by it, the exponential voltage by A, and the exponential capacity by B. The next subsections elaborate on the mathematical models of dynamic systems. Detailed explanations of each model are provided, including information on its salient features and an appropriate mathematical model.

Mathematical formulation of a statistic model

A novel multi-level PFC EV wireless charging system transforms electric vehicle charging. Its innovative converter architecture, intelligent control algorithms, and wireless charging provide ease, power transfer efficiency, and power grid integration. This technology enables a sustainable future where electric mobility replaces fossil fuels and cleans the environment for future generations. Initially, the load of a PFC circuit is described, which in this case is the wireless charging system for EVs. The state space model analysis is using a boost converter-based power factor correction (PFC) circuit [34–36].

$$\begin{bmatrix} \frac{dx_1}{dt} \\ \frac{dx_2}{dt} \\ \frac{dx_3}{dt} \end{bmatrix} = \begin{bmatrix} 0 & 0 & 0 \\ 0 & 0 & -\frac{1}{C} \\ 0 & \frac{1}{L_2} & -\frac{R}{L_2} \end{bmatrix} \begin{bmatrix} x_1 \\ x_2 \\ x_3 \end{bmatrix} + \begin{bmatrix} \frac{1}{L_1} & 0 \\ 0 & \frac{1}{C} \\ 0 & 0 \end{bmatrix} \begin{bmatrix} U_1 \\ U_2 \end{bmatrix} \tag{5}$$

$$\begin{bmatrix} \frac{dx_1}{dt} \\ \frac{dx_2}{dt} \\ \frac{dx_3}{dt} \end{bmatrix} = \begin{bmatrix} 0 & -\frac{1}{L_2} & 0 \\ \frac{1}{C} & 0 & -\frac{1}{C} \\ 0 & \frac{1}{L_2} & -\frac{R}{L_2} \end{bmatrix} \begin{bmatrix} x_1 \\ x_2 \\ x_3 \end{bmatrix} + \begin{bmatrix} \frac{1}{L_1} & 0 \\ 0 & \frac{1}{C} \\ 0 & 0 \end{bmatrix} \begin{bmatrix} U_1 \\ U_2 \end{bmatrix} \tag{6}$$

Mathematical formulation of dynamic model

By excluding consideration of the magnetic losses and the resistance of the coil, a simplified version of the apparent power that is transferred from L_p to L_s can be determined [37].

$$S_{PS} = -U_{PS}I_S^* = -j\omega M i_P \tag{7}$$

The apparent power that is transferred from L_S to L_P can be determined as following Eq. (8).

$$S_{SP} = -U_{SP}I_P^* = -j\omega M i_S i_P^* \tag{8}$$

where the true power transfer can be presented as follows:

$$P_{PS} = \omega M I_P I_S \sin \varphi_{PS} \tag{9}$$

Dynamic power exchanges occur between the two coils. Consider for the sake of this study that a power transfer from L_p to L_s is taking place. When $\phi_{PS}=\pi/2$, the power that is transferred from L_p to L_s reaches its highest level. The maximum efficiency obtained using dynamic charged system is as follows:

$$\eta_{\max} = \frac{k^2 Q_1 Q_2}{\left(1+\sqrt{1+k^2 Q_1 Q_2}\right)^2} \tag{10}$$

Proposed multi-level PFC boost converter rectifier

The suggested converter setup includes a number of crucial elements. First, the input power is provided by an AC source to the PFC rectifier converter which is fed to the roadside LCC network through a high-frequency inverter which is illustrated in Fig. 4. It is crucial to remember that the LCC network does not move when the power is being transferred. The vehicle's end of the LCC network consists of a battery and a regulated rectifier converter, which manages the flow of power between the network and the battery. The rectifier that is included in the converter that is located on the source side of the system makes it easier for electricity to be transferred from the grid to the battery. After that, the high-frequency converter transforms the DC electricity into AC which operates at a high frequency. Then, the vehicle's side converter, which doubles as a rectifier, receives power wirelessly from the parked charging station and transfers it to the battery.

A power factor correction (PFC) rectifier with multi-levels of enhancement has been proposed as shown in Fig. 5. This rectifier uses three active switches and six diodes, which is a modest tweak from an architecture that was comparable but

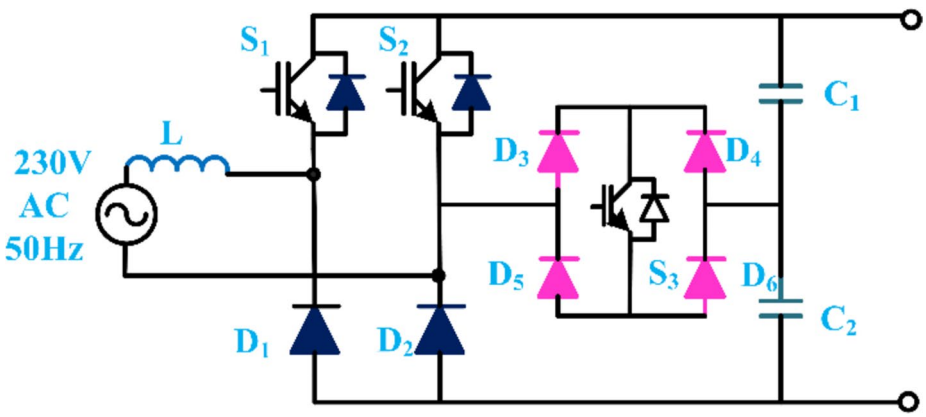

Fig. 4 Proposed multi-level PFC boost converter rectifier

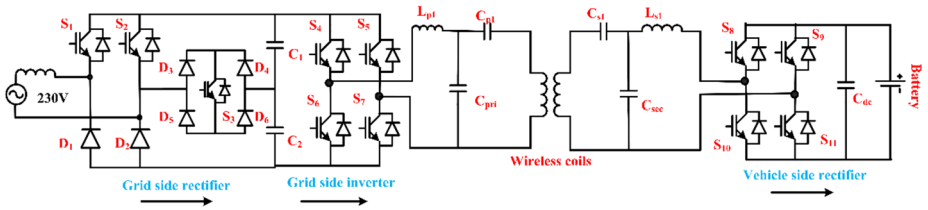

Fig. 5 A two-stage unidirectional EV wireless charging converter

Table 1 Multi-level PFC boost rectifier parameters

System parameters	
Voltage of AC grid	120-V RMS
Frequency of AC grid	60 Hz
Interface inductor	2.5 mH
DC voltages (V_{dc})	200 V
DC capacitor (C_1 & C_2)	1000 µF
Switching frequency	5 kHz

needed four switches. Because of this improvement, there will be less of a need for extra gate drivers, which will save space on the assembled board. Different paths for current are created in proposed controller using midpoint of DC capacitors.

It has five levels of output voltages having $\pm V_{dc}$, $\pm V_{dc}/2$ and 0. When the current is in the positive direction, engaging switch S_1 will cause diode D_2 to conduct. This will result in a voltage of $+V_{dc}$ being present at V_{ab}, and the capacitors C_1 and C_2 will be charged. When switches S_1 and S_3 are both on at the same time, current flows with low impedance via capacitor 1 (C_1) and the bidirectional switch (S_3), charging the top capacitor and bringing V_{ab} up to $+V_{dc}/2$. To get to ground zero, you must use switches S_1 and S_2 to generate a short circuit between locations a and b. Diode D_1 plays a significant part in determining the necessary current route when the current is flowing in the opposite direction, which is negative. When the switch S_3 is activated, all of the current flows through the lower capacitor C_2, charging it, while the other conductor, D_1, is in operation. This results in a negative voltage level of $-V_{dc}/2$ being produced at the input of the rectifier.

Last but not least, when the current is flowing in the opposite direction, engaging switch S_2 causes diode D_1 to conduct, which ultimately results in V_{ab} being equal to $-V_{dc}$. Harmonics are introduced into the current waveform by the voltage waveform of the converter when it is used in an application that is linked to the grid. By using specified parameters in Table 1, the suggested rectifier presents a voltage waveform at the input that has five different levels, which results in decreased harmonic content. As a direct result, grid current drops immediately, and smaller filters may be used in comparison to the standard two-level or two-stage rectifiers. Reduced manufacturing costs are a direct result of the lower size of the passive components, which also contributes significantly to the reduced weight of the converter.

Cascaded inner loop control design

The grid current waveform can be shaped using a method known as hysteresis current control. This method creates a waveform that is similar to a sine wave. On the other hand, it may result in difficulties associated with switching.

As a result of these possible problems, which can involve greater switching losses, increased electromagnetic interference, and the possibility of grid voltage distortion, the design and execution of the control system will need careful attention and the development of techniques to mitigate the effects of these problems. A controller with a straightforward layout has been conceptualized with the goal of making this rectifier topology appealing and suitable for use in industrial settings. The controller is made up of two loops that are cascaded one within the other. The outer loop acts as a voltage regulator, while the inner loop is in charge of controlling the amount of current. Figure 6 displays all of the factors that were considered such as line inductor (L) and parasitic internal inductance (R), α is the rectifier duty cycle, grid current (I_s), and grid voltage (v_s), and output DC voltage (v_s) affects the inner loop control. The mathematical form of inner loop control is expressed as follows:

$$L\frac{di_s}{dt} = v_s - R \times i_s - V_{ab} = v_s - R \times i_s - \alpha V_{dc} \tag{11}$$

By rearranging Eq. (11), the final value of inner loop current controller ($H(s)$) can be represented as follows:

$$H(s) = \frac{i_s}{\alpha} = \frac{-V_{dc}}{LS + R} \tag{12}$$

Cascaded outer loop control design

In continuation, an extra loop, which was formerly known as the outer loop, has to be introduced into the controller so that precise control may be exerted over the DC voltage that is output. It is very necessary to investigate the equations that are associated with the DC side of the rectifier in order to build the system model for this outer loop. For further information on how to calculate the open-loop transfer function ($H^I(s)$) of the whole system, see Fig. 6. Inner loop transfer functions are determined

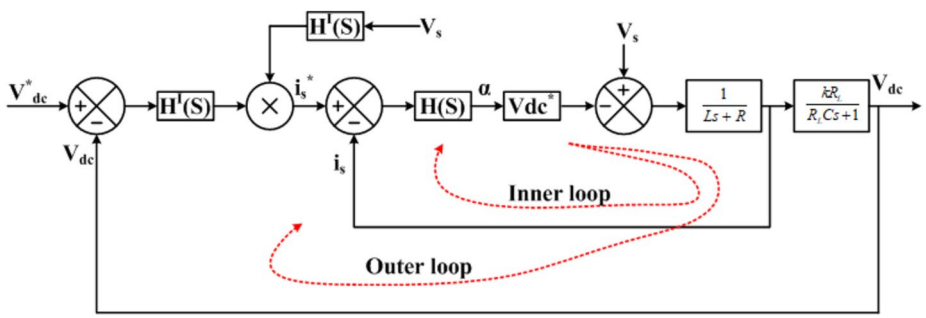

Fig. 6 Cascaded design control block diagram applied on multi-level rectifier

by multiplying the plant model by the compensator *H(s)*, which is a constant. Detailed computations are shown by using a PI controller in the inner loop, although the $k_i c$ has been kept deliberately modest so that the analysis can start with more speed. The constant average value for the duty cycle, indicated by the letter *k*, is becoming closer and closer to the value of unity (getting closer to 1).

The variable i_c stands for the DC capacitor current, and one *C* capacitor is equal to the parallel combination of two C_1 capacitors and two C_1 & C_2 capacitors. It is possible to get the transfer function for the outer loop system by first doing small signal modelling on Eq. (13) and then translating it into the s-plane. This will provide the desired result.

$$\begin{cases} i_f = i_c + i_L \\ i_c = i_f - i_L \\ C\frac{dV_{dc}}{dt} = ki_s - \frac{CV_{dc}}{R_L} \end{cases} \tag{13}$$

The output current control loop ($H^I(S)$) is expressed as follows:

$$H^I(s) = \frac{V_{dc}}{i_s} = \frac{kR_L}{R_L CS + 1} \tag{14}$$

Multicarrier PWM technique

For high-power as well as industrial uses that need a set switching frequency at a low rate, the PWM technique should be used to make the necessary pulses for switching [38–41]. Other switching methods, like hysteresis, have an adaptable switching frequency that makes annoying noises. As shown in Fig. 7, the four carriers (C_{r1}, C_{r2}, C_{r3}, and C_{r4}) are moved vertically to modify the calculated reference signal (U_{ref}). Each of the carriers is responsible for making pulses that match the voltage level as well as switching states shown by logical blocks. The suggested method makes sure that the switching frequency of the multi-level PFC boost rectifier converter is low and set. This is done to get low switching losses while maintaining excellent efficiency compared to other schemes.

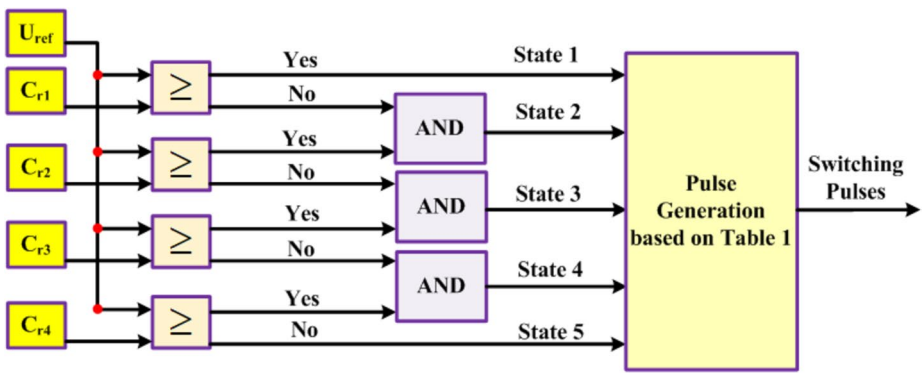

Fig. 7 The low and constant switching frequency applications of the proposed multicarrier PWM approach

Results and discussion

The unidirectional converter for wireless power transfer (WPT) involving the proposed multi-level PFC boost rectifier has been tested in MATLAB 2023a employing the parameters described in Table 1, and the outcomes at different places are shown. The unidirectional converter consists of a multi-level boost PFC rectifier with the DC link. The rectifier receives electricity from the grid at 230 V and 50 Hz, and its operation is synchronized with i_s, assuring a unity power factor.

In Fig. 8, that diagram depicts a low-harmonic, multi-level voltage waveform at the PFC rectifier's input. A high-frequency (HF) inverter is connected to the DC link, and this HF inverter converts DC to AC and fed to transformer via LCC network. LCC network eliminates the ripple in voltage and current, which is then sent to a high-frequency transformer that acts as the wireless power transfer.

The secondary transformer is incorporated into the car, and an LCC resonance network is used to smooth out the voltage and current noise. The output signal of the LCC resonant network is sent to H bridge-controlled rectifier, which charges the EV battery. Figure 9 shows the patterns of the source's voltage and current, which shows that the source's power factor is approximately one. In this case, the source is a single-phase AC supply with 230-V power and 50-Hz frequency. About 20 A of current is taken from the source. In Fig. 10, the voltage and current of the DC link are shown as waveforms. The DC link is connected to the HF inverter which is fed to roadside winding where the power transfer takes place. Here, the power is transferred to the vehicle side winding which is fed to the vehicle rectifier which is fed to the battery.

These waveforms provide an understanding of the characteristics of the source and the DC link in the AC-DC bidirectional wireless power transfer system. They offer insights into the voltage and current levels involved in the conversion process, aiding in the

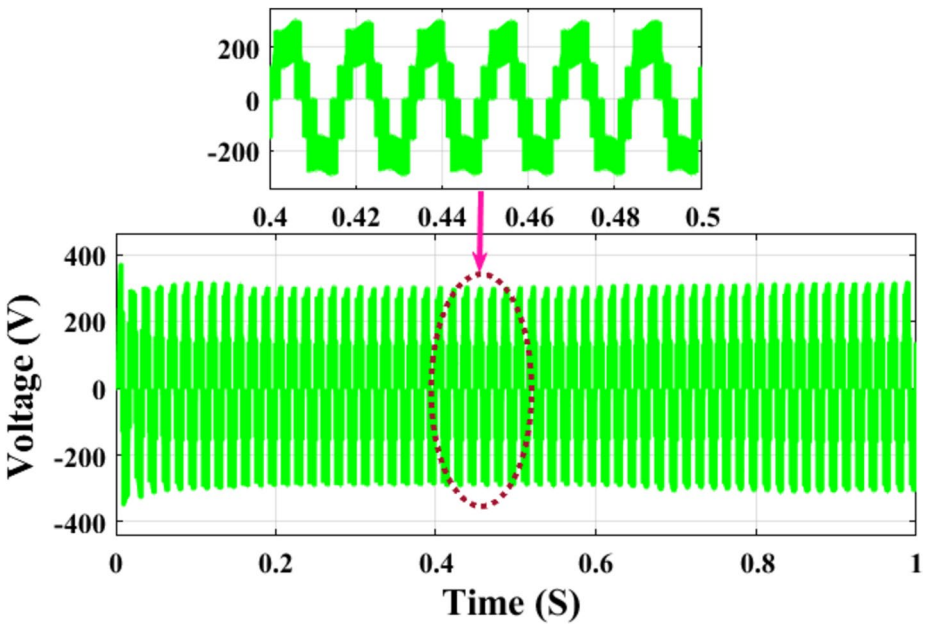

Fig. 8 Multi-level voltage at PFC rectifier input side

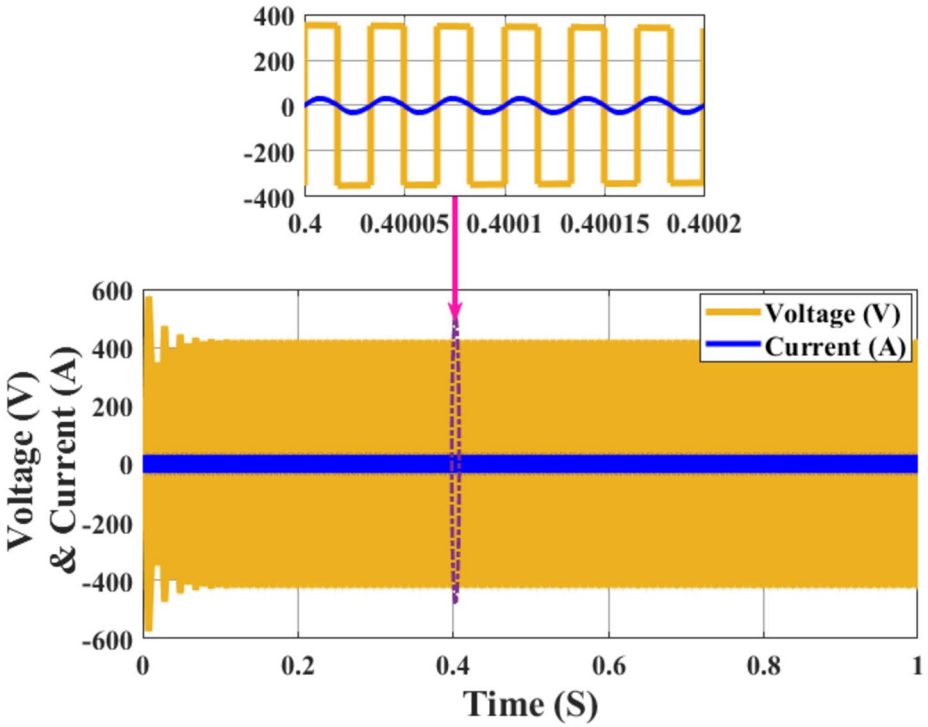

Fig. 9 Voltage and current waveforms of the source

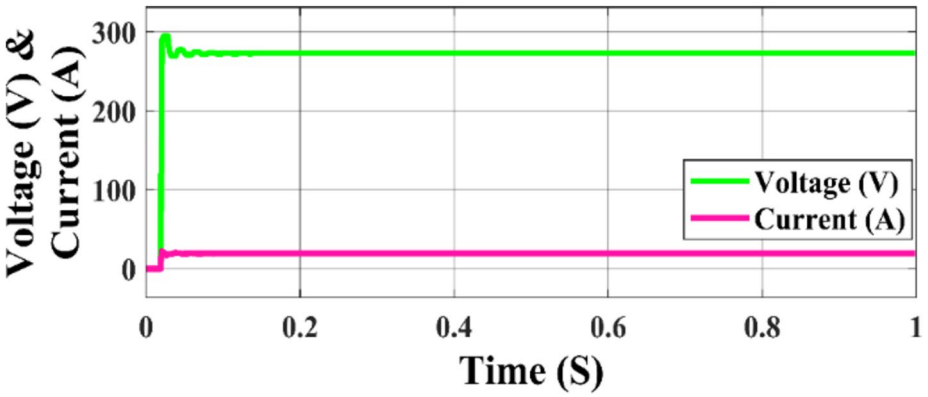

Fig. 10 DC link voltage and DC link current

assessment of system performance, efficiency, and power transfer capabilities. Figure 11 shows the voltage and current on the high-frequency inverter side, and Fig. 12 shows the voltage and current on the vehicle side of the LCC. The DC link sends its output to the high-frequency inverter, which changes the DC into high-frequency AC. The voltage and current of high-frequency AC are 410 V and 13 A, respectively. The high-frequency AC from the wireless transformer is sent to the LCC network in the vehicle, where the waves are smoothed out.

The high-frequency AC is then turned into DC by the vehicle side rectifier and used to charge the E-vehicle's battery. Figure 13 shows that the current for charging the battery is 13 A, and that the voltage for fast charging is about 400 V.

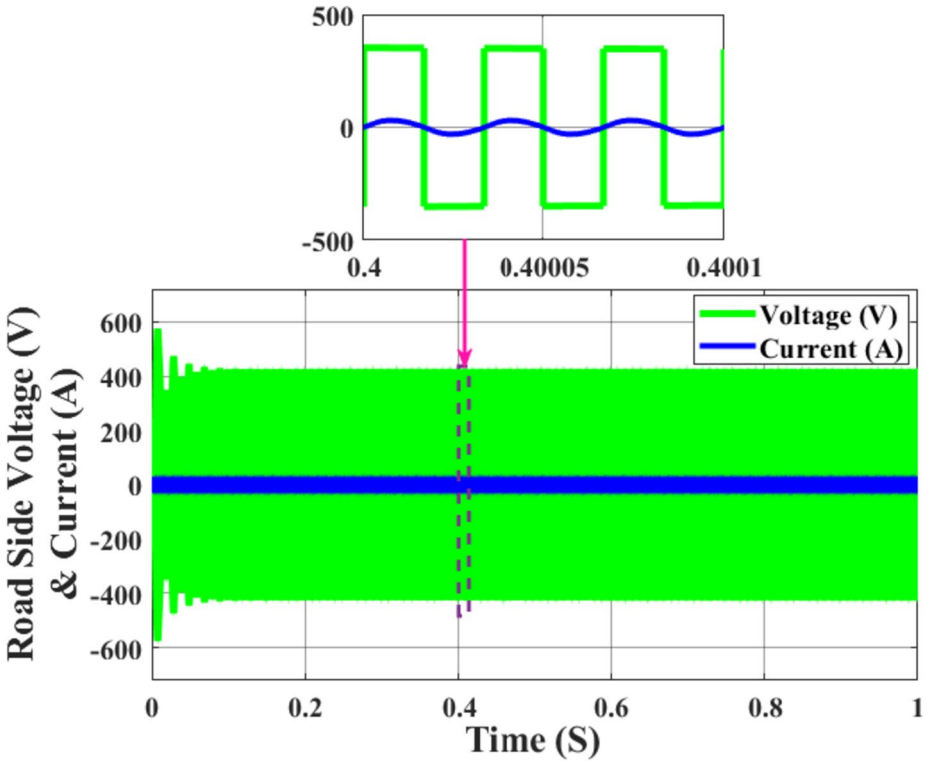

Fig. 11 Inverter side voltage and current waveforms

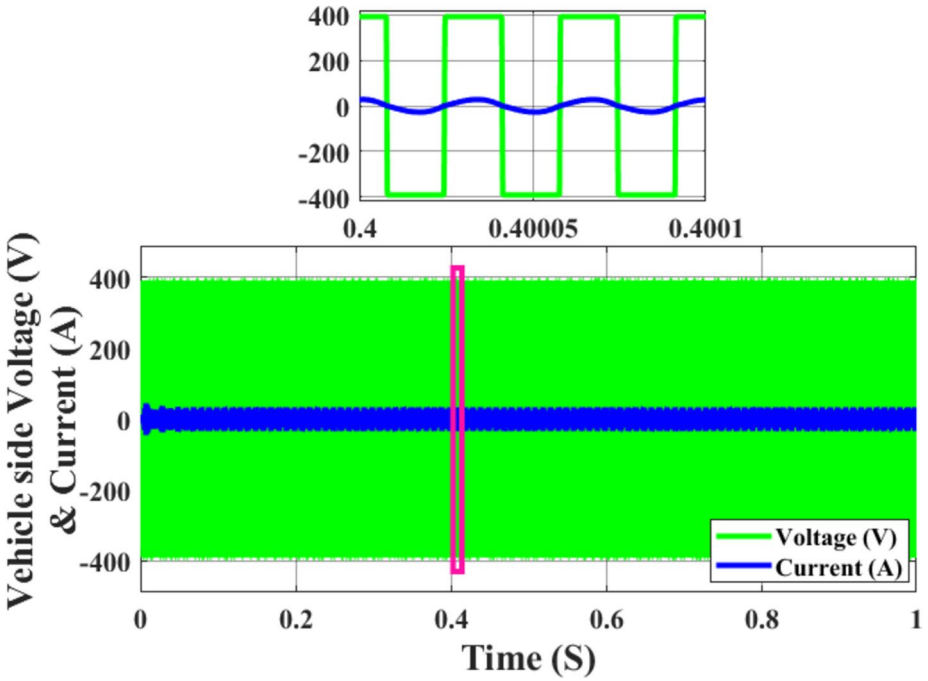

Fig. 12 Voltage and current waveforms on vehicle side

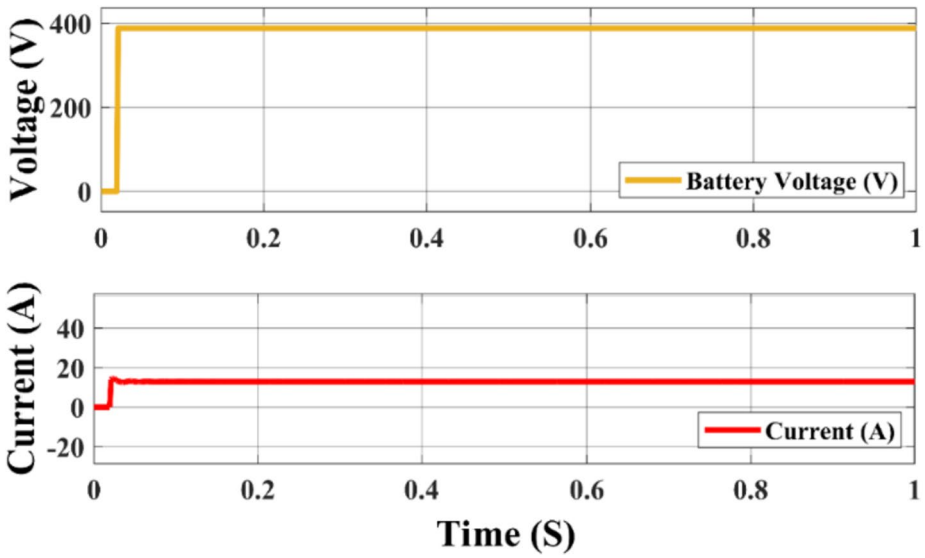

Fig. 13 Battery voltage and current

Experimental

To validate the simulation results, an experiment is done with hardware setup of the wireless power transfer with a multi-level PFC boost rectifier converter which was built using SiC MOSFETs and quick recovery SiC diodes which are depicted in Fig. 14. On an OPAL-RT, the proposed controller as well as modulation method has been used to make pulses for the switches. On the grid side, the voltage and current patterns show that the rectifier is working with a unity power factor. The suggested approach has made it so that the AC current going into the PFC converter has fewer harmonics which is sent to HF inverter.

HF inverter gives the high-frequency AC from the DC link voltage and then sends it to transformer which is again fed to the LCC network to smooth out any waves before the H bridge turns it back into DC. Figure 15 shows the patterns of the experiment's outputs that went with them. Table 2 contrasts the proposed approach with existed topologies, signifying its higher performance along many critical metrics. The proposed technique is effective because it improves charger capability in many ways, including number of levels, active switches, wireless capability, efficiency, power factor, and voltage stress on switches.

In order to convert the voltage from the source into usable current, PFC boost rectifier system needs a voltage source. The potential for current flow is supplied by the source voltage. Current in this configuration is the flow of charge through the PFC boost rectifier circuit, which is driven by the source voltage. To enhance power factor and efficiency, the input alternating current (AC) is rectified into direct current (DC) by the rectifier. Figure 15 a represents the reactive power and maximizes energy utilization to guarantee a steady and efficient flow of electricity to the linked load. The DC link voltage seen in Fig. 15 b in a PFC boost rectifier is the stabilized voltage across the DC capacitor that rounds off the rectifier's output. It keeps the voltage to the devices farther down the line stable. The DC capacitor acts as a buffer between

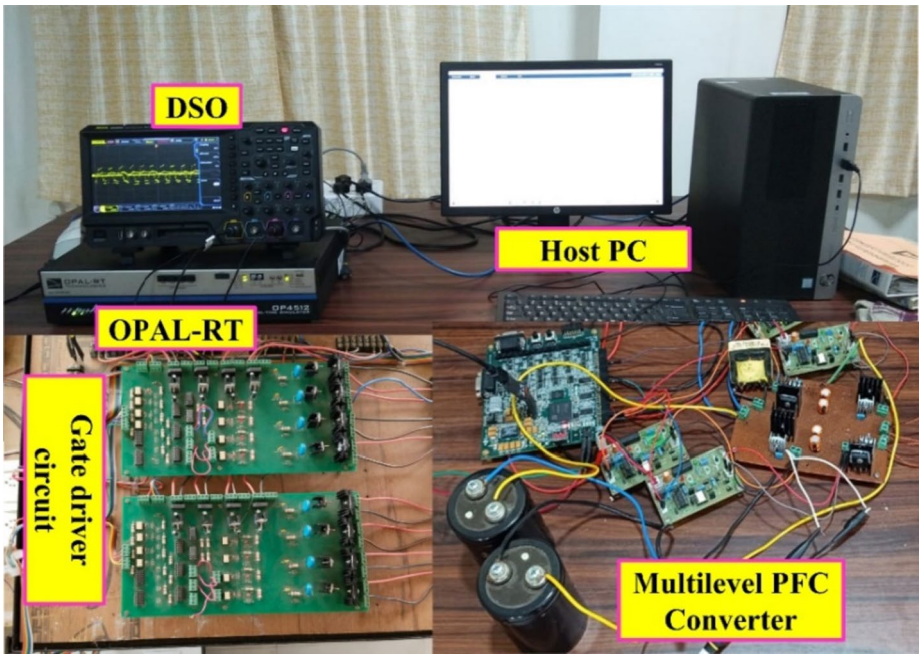

Fig. 14 Experiment setup

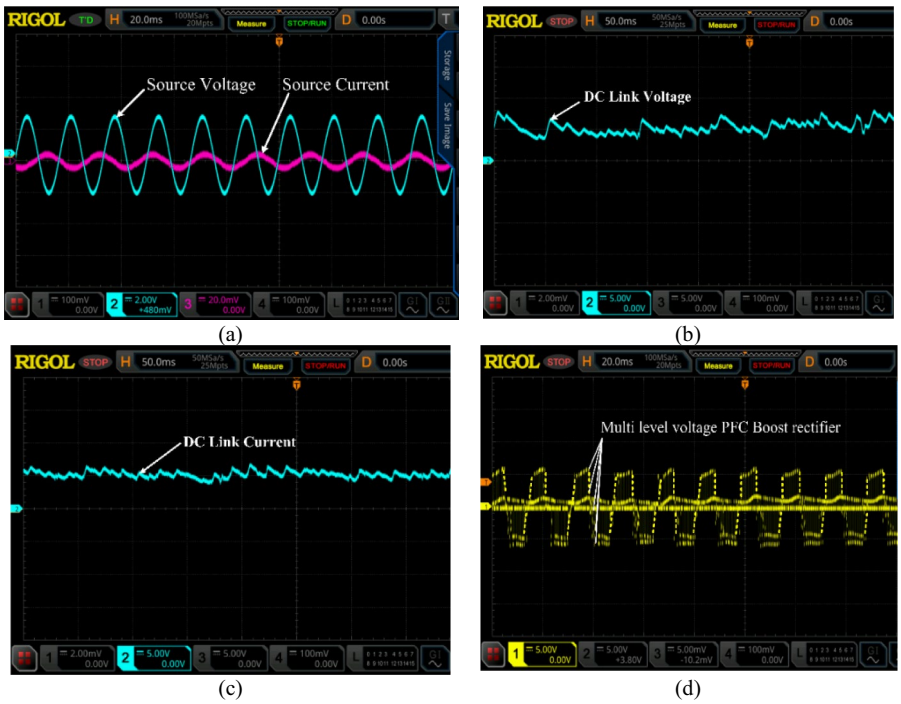

Fig. 15 Experimental validation of proposed multi-level PFC boost converter. **a** Source voltage and current, **b** DC link voltage, **c** DC link current, and **d** multi-level input voltage of proposed PFC boost rectifier

Table 2 The novelty of proposed work is compared with standard topologies

Parameters	[42]	[43]	[44]	[45]	[46, 47]	Proposed
Level	5	5	7	3	3	5
Active switches	6	10	10	4	8	3
Diodes	-	-	-	4	2	6
Inductors	1	1	1	1	1	1
Capacitors	2	3	3	2	4	2
Wireless capability	No	No	No	No	No	Yes
Voltage stress	Less	Less	Less	Less	Less	Very less
Efficiency	94.33%	97.75%	-	90.8%	99.18%	97.2%
Power factor	Unity	Unity	Unity	Unity	0.99	Unity

the input and the output, smoothing out voltage and current spikes and boosting the power factor.

This is represented by the DC link current as shown in Fig. 15 c. PFC boost rectifiers rely on a stable DC link voltage and current for optimal power conversion, lower harmonics, and better system performance. The proposed PFC boost rectifier employs a multi-level input voltage approach. This design strategy involves varying the input voltage levels to the boost converter in a controlled manner. By adjusting these levels from Fig. 15 d, the rectifier aims to achieve improved power factor correction (PFC) performance. This multi-level input voltage technique helps optimize the energy conversion process by minimizing harmonic distortions and enhancing overall power efficiency, contributing to better utilization of input power while meeting PFC requirements.

Conclusions

This research presents modelling and experimental validation of a novel multi-level PFC converter that has reduced switch count for unidirectional wireless power transmission for charging the batteries of electric vehicles. To maintain DC voltage regulation and input AC voltage and current unity power factor mode, a cascaded PI controller was developed. In addition, by using a modest inductive filter on the input line and the built controller, we were able to generate a low-harmonic AC current waveform. The value of the voltage THD is also lowered to 1.57%. In this study, we employ a multicarrier modulation strategy and use pulse-width modulation to lower the switching frequency, which is a major problem with switching rectifiers. The ripple in the DC is controlled by the DC-link capacitor. Power may thus efficiently flow from the grid to EVs. With an input voltage of 230 V, an output battery voltage of 400 V, and a resonance frequency of 25 kHz, the minimum power from vehicle to grid is 5 kW. Because of the high frequency, the inductor and capacitor used to store energy may be made smaller and lighter. A 97.2% efficiency was measured for the grid-to-battery converter in the car.

Nomenclature

U_{batt}	Battery voltage (V)
$U_{batt\text{-}charge}$	Battery voltage during charging (V)
$U_{batt\text{-}discharge}$	Battery voltage during discharging (V)
E_b^I	Charge and discharge voltage (V)

$q(t)$	Battery's remaining capacity (Wh)
$q(0)$	Initial battery capacity (Wh)
η_{bat}	Battery performance
I_{batt}	Battery current (A)
R_{batt}	Internal resistance of battery (Ω)
q_{max}	Maximum battery capacity
E_0	Battery constant voltage (V)
K_b	Polarization resistance (Ω)
t_{batt}	Battery discharge time (s)
i_{ld}^*	Low frequency current dynamics
A	Exponential voltage (V)
B	Exponential capacity (Wh)
x_1, x_2, x_3	State vectors
$dx_1/dt, dx_2/dt, dx_3/dt$	Rate of change of state vectors
R, L_1, L_2, C	Resistance, inductance, and capacitance of PFC converter
U_1, U_2	Output vector
S_{PS}	Apparent power exchanged from primary to secondary winding (VA)
U_{PS}	Coil voltage from primary to secondary winding (V)
I_S^*	Dynamic secondary side coil current (A)
ω	Angular velocity (rad)
M	Mutual inductance (H)
i_P	Primary coil side current (A)
S_{SP}	Apparent power exchanged from primary to secondary winding (VA)
U_{SP}	Coil voltage from secondary to primary winding (V)
I_P^*	Dynamic primary side coil current (A)
I_s	Secondary coil current (A)
P_{PS}	Active power from primary to secondary coil side (W)
ϕ_{PS}	Phase angle between primary and secondary side (rad)
η_{max}	Maximum performance of PFC converter
Q_1, Q_2	Quality factors
k	Coupling factor
S_1, S_2, S_3, S_4, S_5 $S_6, S_7, S_8, S_9, S_{10}, S_{11.}$	MOSFET switches
$D_1, D_2, D_3, D_4, D_5, D_6$	Diodes in PFC converter
C_1, C_2	Capacitances in PFC converter (F)
C_{dc}	DC link capacitor (F)
L	Line inductor (H)
L_{P1}, L_{S1}	Primary and secondary coil inductances (H)
C_{P1}, C_{S1}	Primary and secondary side capacitances (F)
C_{Pri}, C_{sec}	Capacitance across primary and secondary winding (F)
$H(s)$	Transfer function for inner loop current controller
$H^I(s)$	Transfer function for outer loop current controller
V_s	Grid voltage (V)

i_s	Grid current (A)
V_{dc}	DC voltage output (V)
V_{dc}^{*}	Dynamic DC voltage output (V)
R	Parasitic internal resistance (Ω)
α	Rectifier duty cycle
U_{ref}	Reference signal
C_{r1}, C_{r2}, C_{r3}, C_{r4}	Carrier signals

Abbreviations

WPT	Wireless power transfer
PFC	Power factor correction
EV	Electric vehicle
ICE	Internal combustion engines
OBC	Onboard charging
PWM	Pulse-width modulation
BEV	Battery electric vehicle
HF	High frequency

Acknowledgements
Not applicable

Authors' contributions
OD manuscript preparation and writing, SP results editing, JVGRR data collection and manuscript editing, PK manuscript sketch work and software simulation work.

Funding
There is no funding body involved in this article.

Availability of data and materials
Figures: Microsoft Visio 2007, Microsoft Excel, tables: Microsoft Word, and simulation software: MATLAB/Simulink.

Declarations

Ethics approval and consent to participate
We declare that this manuscript is original, has not been published before, and is not currently being considered for publication elsewhere, and there are no conflicts of interest for this publication. As the corresponding author, we confirm that the manuscript has been read and approved for submission by all the named authors.

Competing interests
The authors declare that they have no competing interests.

Received: 28 August 2023 Accepted: 8 December 2023
Published online: 03 January 2024

References

1. IEA (2021) Global EV Outlook 2021. IEA, Paris https://www.iea.org/reports/global-ev-outlook-2021
2. Zhang Z, Pang H, Georgiadis A, Cecati C (2019) Wireless power transfer—an overview. IEEE Trans Ind Electron 66(2):1044–1058
3. Wu M et al (2022) A compact coupler with integrated multiple decoupled coils for wireless power transfer system and its anti-misalignment control. IEEE Trans Power Electron 37(10):12814–12827
4. Y. Zhang et al., "Integration of onboard charger and wireless charging system for electric vehicles with shared coupler, compensation, and rectifier," IEEE Trans. Ind. Electron., to be published, DOI: https://doi.org/10.1109/TIE.2022.3204857
5. Shi K, Tang C, Long H, Lv X, Wang Z, Li X (2022) Power fluctuation suppression method for EV dynamic wireless charging system based on integrated magnetic coupler. IEEE Trans Power Electron 37(1):1118–1131
6. Li G, Ma H (2022) A hybrid IPT system with high-misalignment tolerance and inherent cc–cv output characteristics for EVs charging applications. IEEE J Emerg Sel Topics Power Electron 10(3):3152–3160
7. Hui SY (2013) Planar wireless charging technology for portable electronic products and QI. Proc IEEE 101(6):1290–1301
8. Tang SC, Lun TLT, Guo Z, Kwok K, Mcdannold NJ (2017) Intermediate range wireless power transfer with segmented coil transmitters for implantable heart pumps. IEEE Trans Power Electron 32(5):3844–3857
9. Y. Zhang et al., "Passive paralleling of multi-phase diode rectifier for wireless power transfer systems," IEEE Trans. Circuits Syst II, Exp. Briefs, to be published, doi: https://doi.org/10.1109/TCSII.2022.3215465

10. Ahmad A, Alam MS, Chabaan R (2018) A comprehensive review of wireless charging technologies for electric vehicles. IEEE Trans on Transp Electrific 4(1):38–63
11. Triviño A, González-González JM, Aguado JA (2021) Wireless power transfer technologies applied to electric vehicles: a review. Energies 14(6):1547. https://doi.org/10.3390/en14061547
12. Sharma A, Sharma S (2019) Review of power electronics in vehicle-togrid systems, pp 337–361
13. Trivino A, Gonzalez-Gonzalez JM, Castilla M (2021) Review on control techniques for EV bidirectional wireless chargers. Electronics 10(16):1905. Available: https://www.mdpi.com/2079-9292/10/16/1905/htm, https://www.mdpi.com/2079-9292/10/16/1905
14. Lee I-O, Moon G-W (2014) Half-bridge integrated ZVS full-bridge converter with reduced conduction loss for electric vehicle battery chargers. IEEE Trans Ind Electron 61(8):3978–3988
15. Das D, Weise N, Basu K, Baranwal R, Mohan N (2019) A bidirectional soft-switched DAB-based single-stage three-phase AC–DC converter for V2G application. IEEE Transactions on Transportation Electrification 5(1):186–199. https://doi.org/10.1109/TTE.2018.2886455
16. Gupta J, Kushwaha R, Singh B, Khadkikar V (2022) Improved power quality charging system based on high step-down gain bridgeless SEPIC APFC for light electric vehicles. IEEE Trans Ind Appl 58(1):423–434. https://doi.org/10.1109/TIA.2021.3120028
17. Oh CY, Kim DH, Woo DG, Sung WY, Kim YS, Lee BK (2013) A high-efficient nonisolated single-stage on-board battery charger for electric vehicles. IEEE transactions on Power Electronics 28(12):5746–5757
18. Sreehari P, Kumar NB, Ismayil C (2023) Two stage EV charger based on bridgeless PFC converter for e-Rickshaw. 2023 International Conference on Power, Instrumentation, Control and Computing (PICC), Thrissur, India, pp 1–5. https://doi.org/10.1109/PICC57976.2023.10142594
19. Dixit A, Pande K, Gangavarapu S, Rathore AK (2020) DCM-based bridgeless PFC converter for EV charging application. IEEE Journal of Emerging and Selected Topics in Industrial Electronics 1(1):57–66. https://doi.org/10.1109/JESTIE.2020.2999595
20. Zhao Z, Davari P, Lu W, Blaabjerg F (2023) Online DC-link capacitance monitoring for digital-controlled boost PFC converters without additional sampling devices. IEEE Transactions on Industrial Electronics 70(1):907–920. https://doi.org/10.1109/TIE.2022.3153825
21. Sharifi S, Monfared M, Babaei M (2020) Ferdowsi rectifiers—single-phase buck-boost bridgeless PFC rectifiers with low semiconductor count. IEEE Transactions on Industrial Electronics 67(11):9206–9214. https://doi.org/10.1109/TIE.2019.2955430
22. Latif S, Irshad S, Ahmadi Kamarposhti M, Shokouhandeh H, Colak I, Eguchi K (2022) Intelligent design of multi-machine power system stabilizers (PSSs) using improved particle swarm optimization. Electronics (Basel) 11(6):946
23. Kamarposhti MA, Lesani H (2011) Effects of STATCOM, TCSC, SSSC and UPFC on static voltage stability. Electr. Eng. (Berl., Print) 93(1):33–42
24. Abul'Wafa AR (2011) Reliability/cost evaluation of a wind power delivery system. Electric Power Syst Res 81(4):873–879
25. Ahmadi Kamarposhti M (2018) Optimal control of islanded micro grid using particle swarm optimization algorithm. International Journal of Industrial Electronics Control and Optimization 1(1):53–60
26. Kamarposhti MA, Mozafari SB, Soleymani S, Hosseini SM (2015) Improving the wind penetration level of the power systems connected to doubly fed induction generator wind farms considering voltage stability constraints. J Renew Sustain Energy 7(4)
27. Shokouhandeh H, Latif S, Irshad S, Ahmadi Kamarposhti M, Colak I, Eguchi K (2021) Optimal management of reactive power considering voltage and location of control devices using artificial bee algorithm. Appl Sci (Basel) 12(1):27
28. Ahmadi Kamarposhti M, Shokouhandeh H, Alipur M, Colak I, Zare H, Eguchi K (2022) Optimal designing of fuzzy-PID controller in the load-frequency control loop of hydro-thermal power system connected to wind farm by HVDC lines. IEEE Access 10:63812–63822
29. Mohamed N et al (2022) A new wireless charging system for electric vehicles using two receiver coils. *Ain Shams Eng J* 13(2):101569
30. Wang J et al (2022) Precise equivalent circuit model for Li-ion battery by experimental improvement and parameter optimization. J Energy Storage 52(104980):104980
31. Poopanya P, Sivalertporn K, Phophongviwat T (2022) A comparative study on the parameter identification of an equivalent circuit model for an Li-ion battery based on different discharge tests. World Electric Veh J 13(3):50
32. Karakaş S, Şehirli E (2023) Full bridge DC-DC converter-based battery charger with PFC CUK converter having hysteresis control. In: 2023 5th Global Power, Energy and Communication Conference (GPECOM)
33. Lin F-J, Huang M-S, Yeh P-Y, Tsai H-C, Kuan C-H (2012) DSP-based probabilistic fuzzy neural network control for Li-ion battery charger. IEEE Trans Power Electron 27(8):3782–3794
34. Mohamed N, Aymen F, Alqarni M (2021) Inductive power transmission system for electric car charging phase: modeling plus frequency analysis. World Electric Veh J 12(4):267
35. Krishna SA, Abraham L (2014) Boost converter-based power factor correction for single phase rectifier using fuzzy logic control. In: 2014 First International Conference on Computational Systems and Communications (ICCSC)
36. Sayed SS, Massoud AM (2022) Review on state-of-the-art unidirectional non-isolated power factor correction converters for short-/long-distance electric vehicles. IEEE Access 10:11308–11340
37. Mahesh A, Chokkalingam B, Mihet-Popa L (2021) Inductive wireless power transfer charging for electric vehicles–a review. IEEE Access 9:137667–137713
38. McGrath BP, Holmes DG (2002) Multicarrier PWM strategies for multilevel inverters. IEEE Trans Ind Electron 49:858–867
39. Holmes G, Lipo T (2003) Pulse width modulation for power converters: principles and practice. IEEE Press

40. Sushama M, Kumar PS, Reddy CL (2018) Implementation and performance analysis of cascaded multilevel inverter using modified SVPWM techniques. Int J Power Electron 9(3):250
41. Lokeshwar Reddy C, Sree Lakshmi G (2022) Design of cascaded multilevel inverter-based STATCOM for reactive power control with different novel PWM algorithms. In: Lecture Notes in Electrical Engineering. Springer Nature Singapore, Singapore, pp 1033–1053
42. Barwar MK, Kumar Sahu L, Bhatnagar P, Tripathi PR (2022) A multilevel PFC rectifier with sensor-less voltage balancing capability. IEEE Transactions on Circuits and Systems II: Express Briefs 69(12):5029–5033. https://doi.org/10.1109/TCSII.2022.3199088
43. Jain A, Gupta KK, Jain SK (2023) a novel single/multiple output multilevel buck rectifier for EV-battery charging. IEEE Transactions on Vehicular Technology 72(4):4384–4393. https://doi.org/10.1109/TVT.2022.3222349
44. Jain A, Agarwal R, Gupta KK, Jain SK (2022) A V2G-enabled seven-level buck PFC rectifier for EV charging application. 2022 24th European Conference on Power Electronics and Applications (EPE'22 ECCE Europe), Hanover, Germany, pp 1–10
45. Dusmez S, Li X, Akin B (2014) A single-stage three-level isolated PFC converter. 2014 IEEE Energy Conversion Congress and Exposition (ECCE), Pittsburgh, PA, USA, pp 586–592. https://doi.org/10.1109/ECCE.2014.6953447
46. Xiong K et al (2019) 5-level flying capacitor bridgeless PFC converter using cost-effective low-voltage GaN transistors. 2019 IEEE Energy Conversion Congress and Exposition (ECCE), Baltimore, MD, USA, pp 187–192. https://doi.org/10.1109/ECCE.2019.8912751
47. Lachvajderova L, Kadarova J (2021) Analysis of internal combustion engine vehicle, battery electric vehicle and emissions from transport. Transp Logistics 21:21–33

Publisher's Note